# SAM, the SOR Atmospheric Monitor

**Dr. Earl Spillar**
*Air Force Research Laboratory Optics Division*

**Marjorie Shoemake**
*Air Force Research Laboratory Optics Division and the Boeing Corporation*

**Ann Slavin**
*Air Force Research Laboratory Optics Division and the Boeing Corporation*

## ABSTRACT

We describe the Starfire Optical Range Atmospheric Monitor (SAM). SAM is designed to measure the Fried coherence length $r_0$, the Greenwood frequency $f_G$, and the isoplanatic angle $\theta_0$ even in relatively poor conditions ($r_0 \sim 1$ cm) with high accuracy $\sim 10\%$ with a single frame of data. In addition, since SAM is based on a Shack-Hartmann wave front sensor, more sophisticated statistics about the wave front and the atmosphere should be able to be recovered from the data with additional processing.

## 1. INTRODUCTION

Many different methods of measuring atmospheric turbulence have been used over the years ([1], [2], [3], [4]). The Starfire Optical Range Atmospheric Monitor (SAM) was designed to help us understand the characteristics of the atmosphere when turbulence conditions are poor, such as during the day, and to also gather "higher order" information for wavefront statistics not normally calculated by typical $r_0$ meters.

In order to collect even under severe conditions, SAM incorporates a Shack-Hartmann wave front sensor with small (2 cm) subpertures. This enables SAM to measure values of $r_0$ somewhat smaller than 2 cm. Moreover, we should be able to estimate even smaller values when we enable the operation of the full $4 \times 4$ array of camera pixels associated with each subaperture.

The collection of "higher-order" information is enabled by our Shack-Hartmann wave front sensor (WFS). Because of the large number of subapertures, we collect a statistically significant sample of tilts during each frame, enabling rapid estimation of $r_0$, and hence the ability to detect rapid changes in $r_0$. In addition, using a Shack-Hartmann WFS enables us to measure not just a few separations as are sampled by a differential image motion sensor, but many separations simultaneously. We intend to leverage this information to make measurements of deviations from the Kolmogorov model, and also to enable the measurement of different atmospheric layers as described below.

## 2. THE INSTRUMENT

The optical tube assembly (OTA) for SAM includes a stock 16" Ritchey-Chrétien telescope from RC Optical Systems (RCOS) . The RCOS telescope has a secondary which obscures the inner 31% of the subapertures. The OTA is mounted on a Paramount ME mount. The pointing accuracy for the Paramount ME ranges from 10 to 30 arcseconds after performing a mount model.

SAM is located in a small 10.5 foot dome 16 meters above the top of the hill that is referred to as "Mount Fugate". SAM is situated a few meters from the 1.5 m and 3.5 m site telescopes. Fig. 1 is a picture of SAM.

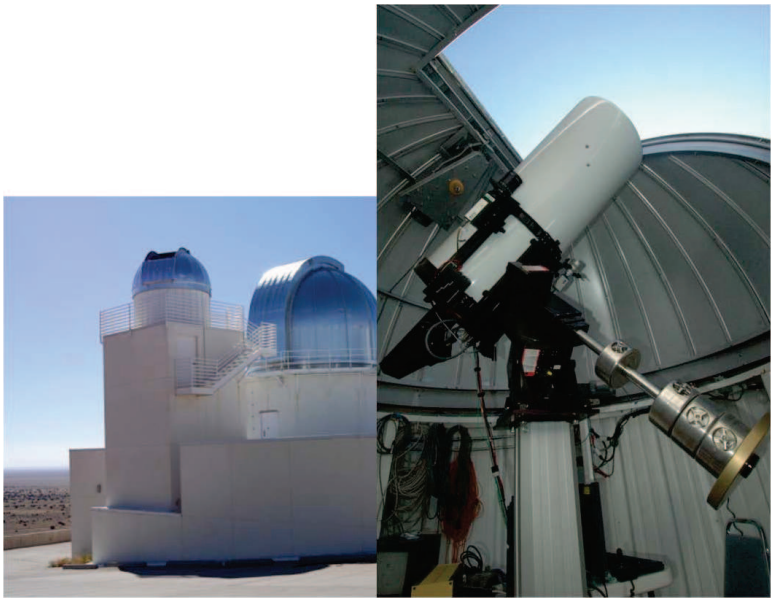

**Fig. 1. Dome location (left), SAM (right).**

## 3. WAVE FRONT SENSOR OPTICS

Light from the RCOS telescope is passed to a custom optics assembly mounted at the Cassegrain back plate of the telescope (a schematic of the optics is shown in Fig. 2). First, a square field stop at the focus of the RCOS eliminates light which might fall onto adjacent subapertures (see Fig. 3). The field stop is slightly undersized, in that it obscures approximately one pixel around each subaperture. The outer ring of pixels is used as a "guard band", and is ignored in all calculations. This limits the magnitude of the tilt that the instrument can accurately measure, and hence the minimum value of $r_0$ that it can measure.

After passing through the field stop, the light is collimated and passes through a filter wheel holding six 1-inch round filters. 500, 600, 650 and 700 nm long pass filters are available; the best filter is selected based on the star selection to maximize the SNR without saturating the detector.

Next an image of the pupil is formed on the lenslet array, which forms $20 \times 20$ subapertures across the pupil of the telescope. Another lens relays the images formed by the lenslet array to the CCD; each lenslet image is formed on $4 \times 4$ pixel elements on the CCD. The field of view for one pixel is $40\mu$rad, while the size of each subaperture is .02m.

The CCD itself is mounted to the optics wedge. The camera and associated electronics are an off the shelf configuration from SciMeasure. The CCD is an $80 \times 80$ pixel CCD-39 from E2V with a read noise of 9 electrons and a peak quantum efficiency of approximately 59%. The camera system is capable of doing full frame reads at a rate of 2kHz; in order to maintain a sufficiently high signal to noise we typically operate at 1kHz, capturing 1000 frames in one second. These frames are saved to HDF5 files for analysis. Typically, a mean value of $r_0$ is calculated using 2000 frames every 45 seconds when SAM is being operated as a facility instrument.

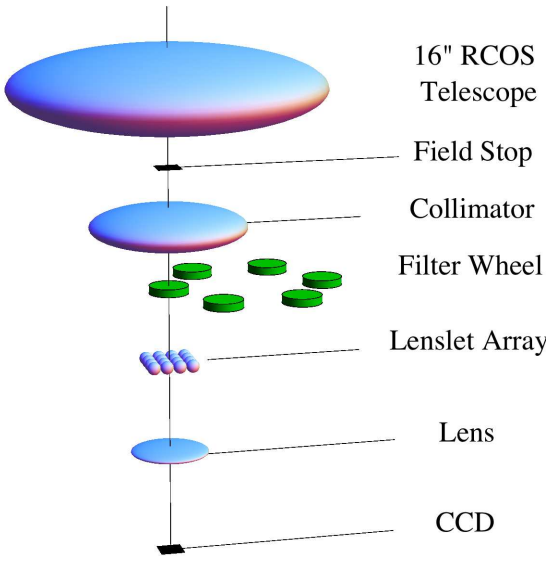


**Fig. 2. Schematic of the Optics. Light travels from the top to the bottom.**

## 4. ESTIMATING $r_0$

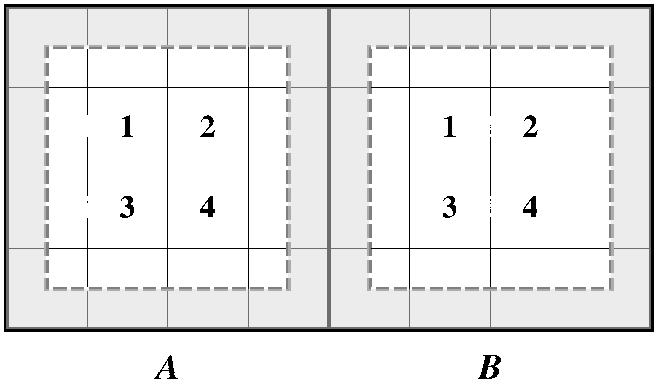


**Fig. 3. Depiction of CCD pixels for two subapertures.**

For the first incarnation of SAM, we estimate the tilt using the differential tilt method, but instead of using a pair or a small number of subapertures, we use many pairs of subapertures across the whole Shack-Hartmann wave front sensor. For now we estimate the value of $r_0$ from the mean differential tilt as discussed in [5], and we only calculate the value of $r_0$ based on adjacent subapertures. We differentiate between 4 different estimates in this paper. First, we take adjacent apertures in either the x direction or the y direction. Second, we can take the difference in the gradient either parallel to, or perpendicular to, the vector separating the two subapertures in question. As we shall see in the results section, these 4 estimates all agree with each

other, as they ought due to the theory presented in [5], which assumes Kolmogorov phase statistics. We first calculate the gradients from the energy imbalances

$$\theta_x = \alpha \frac{I_1 + I_3 - I_2 - I_4}{I_1 + I_3 + I_2 + I_4}.$$

$\alpha$ was calibrated by injecting known tilts in the lab. Given these angles, we calculate the differential tilts

$$\sigma^2_{\perp,A,B} = \langle(\theta_{A,y} - \theta_{B,y})^2\rangle \quad \text{and} \quad \sigma^2_{\parallel,A,B} = \langle(\theta_{A,x} - \theta_{B,x})^2\rangle,$$

where $\langle\cdot\rangle$ represents averaging over several subapertures. Finally these quantities are converted into $r_{0,\perp}$ and $r_{0,\parallel}$ using

$$\sigma^2_{\perp} = 0.1119(l/r_0)^{5/3}(\lambda/l)^2 \quad \text{and} \quad \sigma^2_{\parallel} = 0.0484(l/r_0)^{5/3}(\lambda/l)^2,$$

the formulae found in [5].

The agreement of these 4 statistics (see the next section) represents a very simple confirmation of the Kolmogorov theory. In future work, we will be using other statistics to further test the Kolmogorov hypothesis. For example, by looking at subapertures beyond the adjacent ones, we can test the 5/3 power law of the structure function, and perhaps detect the inner scale in some conditions.

## 5. VALIDATION

We have validated both the algorithms and basic design of SAM against simulations, and validated the basic functionality of SAM against another $r_0$ instrument.

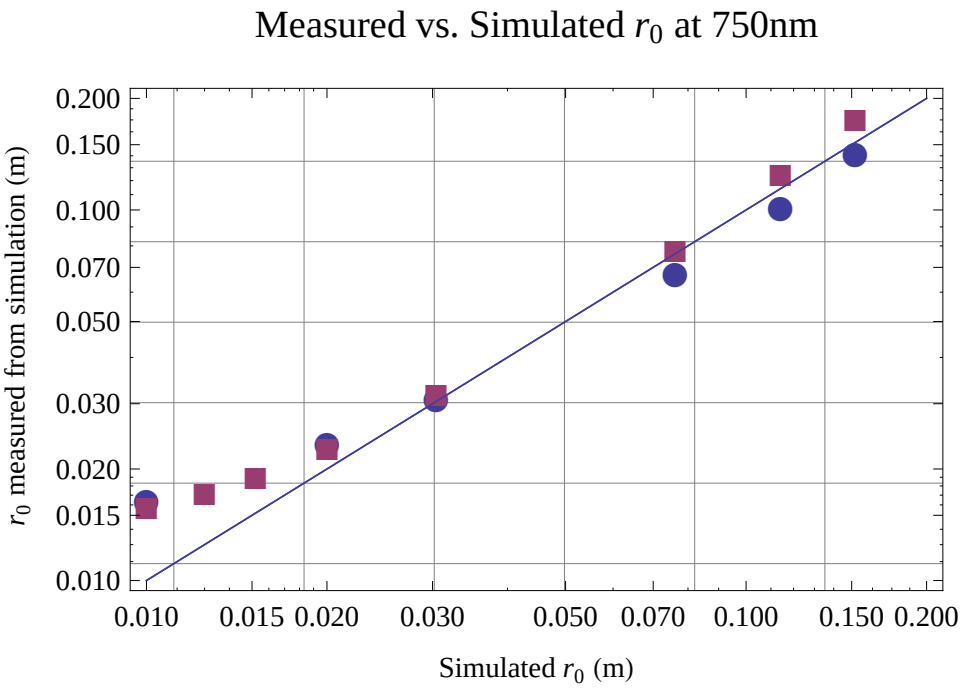


**Fig. 4. Simulation of SAM measurements**

In order to validate the optical and algorithmic design of SAM, we created a wave optics simulation of SAM in the ACS wave optics simulation system. We propagated through a variety of atmospheres, collected simulated data, and ran the data through our algorithms. The results are shown in Fig. 4. The blue circles represent atmospheres with 10 Hz Greenwood frequencies, the red squares 200 Hz Greenwood frequencies. We conclude that the software and hardware systems, as designed, should measure $r_0$ down to small values of $r_0$ even when $f_G$ is quite large.

We also compared SAM $r_0$ measurements from another $r_0$ meter deployed nearby, the "mini-SAM" instrument. mini-SAM estimates $r_0$ from the MTF of the image formed during a short exposure. mini-SAM is known to have biases for large values of $r_0$. In Fig. 5 we compare observations with the two instruments; we see good agreement.

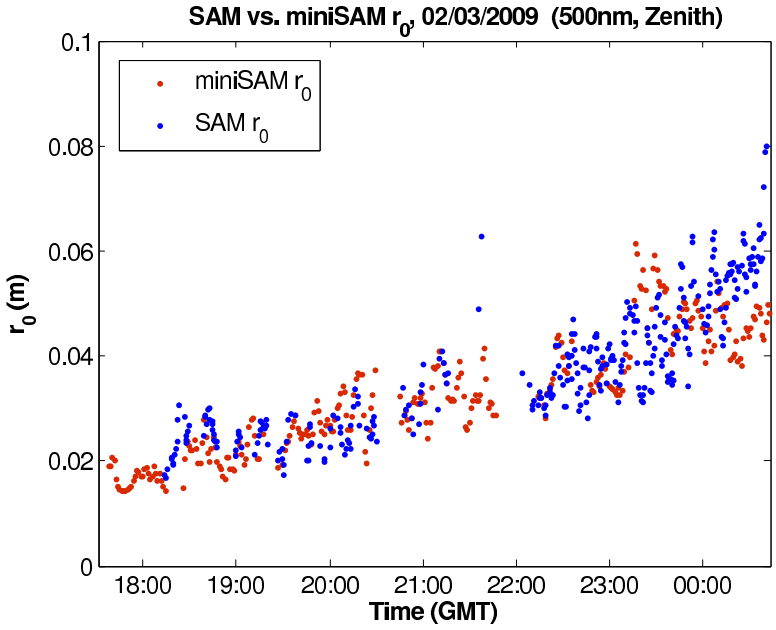


**Fig. 5. Comparison of SAM to mini-SAM.**

## 6. ESTIMATING $\theta_0$

The isoplanatic angle, as defined by Fried [6], weighs the optical turbulence $C_n^2$ with a $z^{5/3}$ altitude dependence:

$$\theta_0 = \left[2.91k^2 \int_0^L C_N^2(z) z^{(5/3)} dz\right]^{-3/5}.$$

Walters and Bradford [7] estimate $\theta_0$ from measurements of the normalized variance of intensity across an aperture:

$$\theta_0 = B\cos^{8/5}(\theta)\left(\frac{\sigma^2}{S^2}\right)^{-3/5}.$$

B refers to a scaling function determined by the size of the aperture calculated in Walters [7]. $\sigma$ is the signal variance of the irradiance across the aperture, while S is the average signal. $\theta_0$ is calculated by summing the signal of each frame, calculating the standard deviation across 2000 frames, and dividing the standard deviation by the average signal for those 2000 frames.

SAMs larger aperture (.4m) follows a quadratic $z^2$ dependence, Fig. 6. To achieve the $z^{5/3}$ scaling the SAM aperture was virtually apodized by .9, creating a smaller aperture.

SAM $\theta_0$ measurements with the apozided filter were once again compared to mini-SAM, Fig. 7. We see good agreement between the instruments.

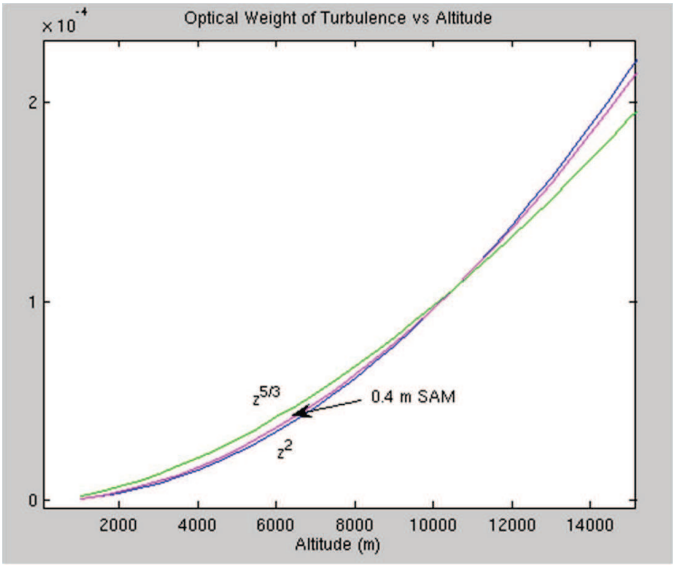


**Fig. 6. $C_N^2$ weights with altitude for SAM and $\theta_0$**

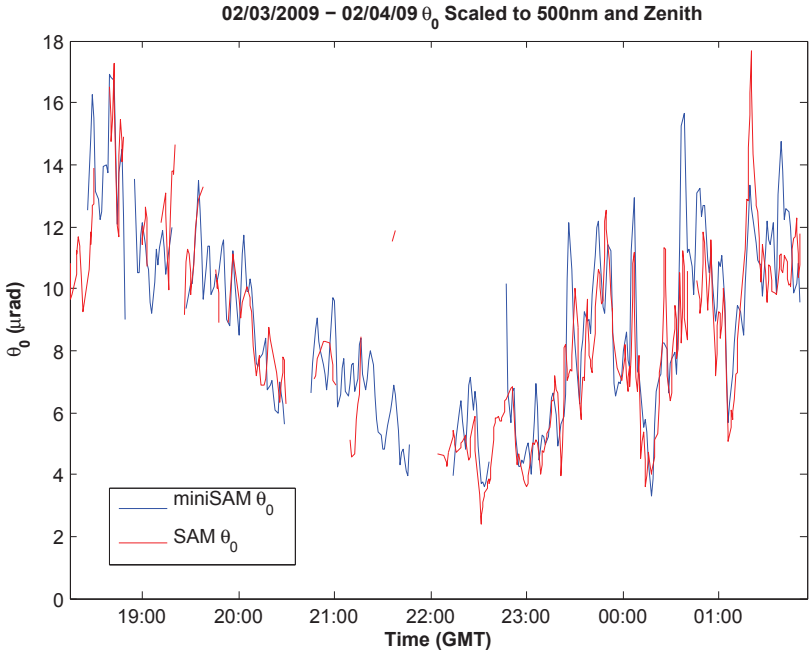


**Fig. 7. $\theta_0$ measurements, SAM and mini-SAM.**

## 7. FROZEN FLOW AND TOMOGRAPHY

Shöck and Spillar [3] demonstrated that the statistics of individual atmospheric layers could be teased out of wave front sensor data. They used data from the 1.5m telescope at SOR, and emphasized the validation of the frozen flow hypothesis. Since SAM is also based on a wave front sensor, it should be possible to repeat and extend this work.

The crux of that work is the observation that if we regard the measured pupil phases (or gradients) as a three dimensional cube of data $\phi(x, y, t)$, and also assume that the frozen flow hypothesis is valid, then

$$\phi_l(x - v_x\tau, y - v_y\tau, t - \tau) = \phi_l(x, y, y)$$

for each frozen layer $l$ for all times $\tau$ so long as $\tau$ is short compared to the time at for which the layer remains frozen. If we take the three dimensional autocorrelation of the data cube, this relation implies that there is a strong autocorrelation along a trajectory

$$(\Delta x, \Delta y, \Delta t) = (v_x t, v_y t, t).$$

These trajectories are visible as "streaks" in the autocorrelation. As the frozen component breaks down, the intensity of the peak decays at larger $t$. If we add more layers, it is easy to see that each contributes its own streak following its own trajectory, under the assumption that each of the random phase screens is independent of the other phase screens. Finally, although we have discussed only the phase screens $\phi(x, y, y)$, other quantities which co-move with the phase screens, including gradient, and intensity fluctuations, also follow the same general behavior.

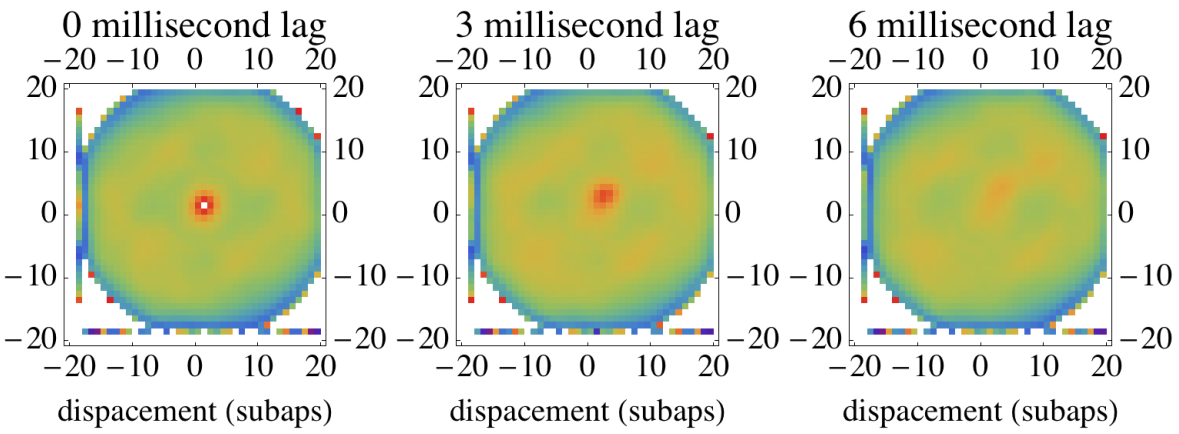


**Fig. 8. Intensity auto correlation of data.**

Using early SAM data, we have reproduced the analysis not with gradients as in [8], but with the *intensity* fluctuations, to produce the data displayed in Fig. 8. We see that the autocorrelation behaves as expected: evidently the wind was blowing in the positive x and positive y direction. (The signal is rather weak partially because of the rudimentary signal processing employed, we believe that further signal processing will tease the signal out.)

Future work will attempt to use a combination of gradient and intensity data to estimate distances to the layers, the speeds and directions of the layers, and the relative intensities of the layers on a second by second basis.

## 8. SAMPLE DATA

In Fig. 9 we display some sample data obtained at SOR with SAM. At the top of the figure we display the value of $r_0$, scaled to zenith and 500nm, for a day, using both $x$ and $y$ separations and $\perp$ and $\parallel$ estimators. Note the excellent agreement between these measures. In the bottom left we plot the standard deviation of the measured values of $r_0$. The standard deviation is calculated as the root mean square of the $r_0$ values which occur during a 2000 frame capture, with a separate $r_0$ calculation being performed on each frame. Note that the error in the estimate in $r_0$ *from a single frame of data* is on the order of 10%. Finally, in the lower left, we display the signal to noise ratio. Note that the signal to noise ratio is quite high. The jumps in the SNR correspond to changes in stars, while the more gradual changes, like that after 13 GMT, correspond to the sun rising.

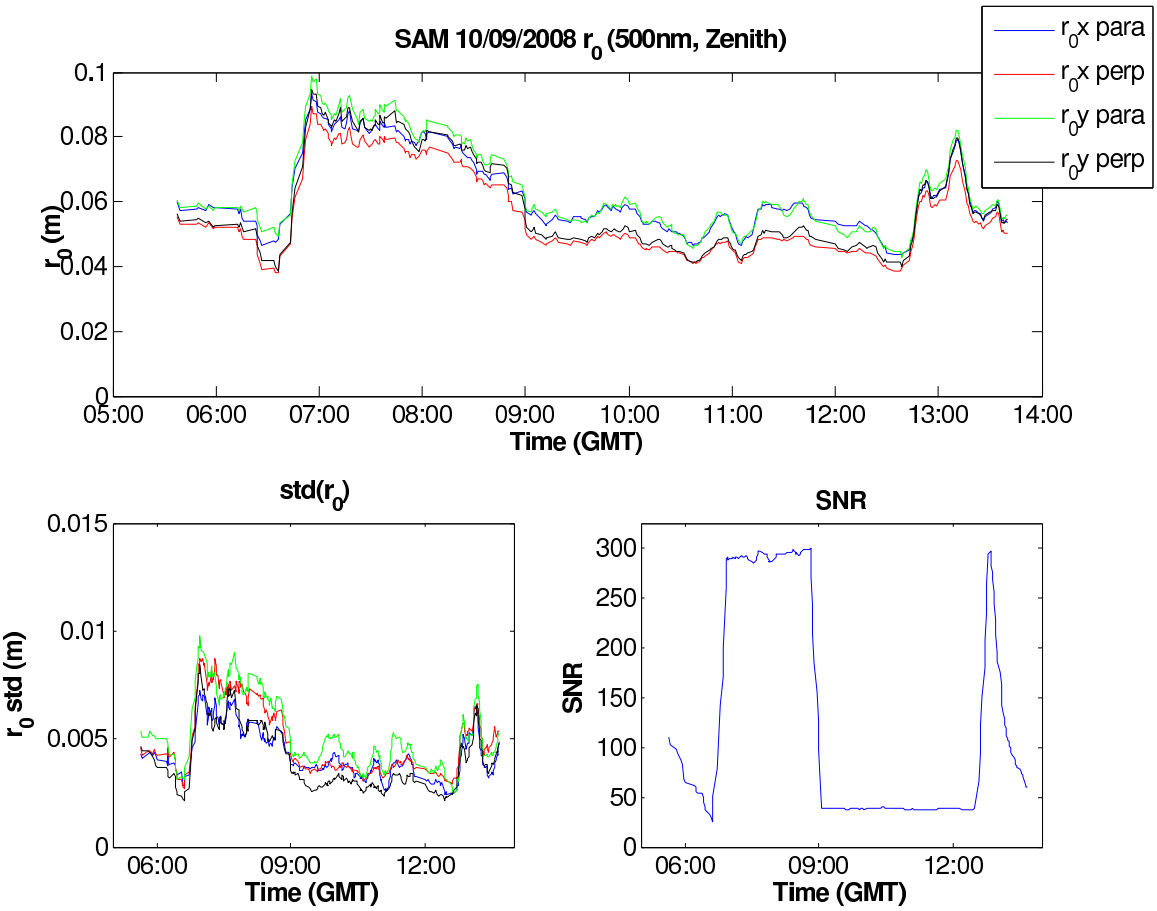


**Fig. 9. Sample observations.**

## 9. CONCLUSIONS

In this paper we have described the Starfire Optical Range Atmospheric Monitor. SAM is currently able to estimate $r_0$ accurately $\pm 10\%$ with a single frame of data, and estimate $\theta_0$ from scintillation values. SAM can operate during both day and night, and operate during relatively severe ($r_0 \approx 1.5$cm) conditions. Finally, we are beginning to use the Shack-Hartmann wave front sensor data to tease apart the layers of turbulence in the atmosphere, and estimate higher order statistics of the wavefront.

## 10. REFERENCES


1. Avila, R., Masciadri, E., Vernin, J., and Sanchez, L. J., Generalized SCIDAR Measurements at San Pedro Martir, *Publications of the Astronomical Society of the Pacific,* 116, 682, 2004.

2. Hickson, P., and Lanzetta, K., Measuring Atmospheric Turbulence with a Lunar Scintillometer Array, *Publications of the Astronomical Society of the Pacific,* 116, 1143, 2004.

3. Tokovinin, A., Optical turbulence profiles at Mauna Kea Measured by MASS and SCIDAR, *Publications of the Astronomical Society of the Pacific,* 114, 1156, 2002.

4. Walters, D., and Brandford, L., Measurements of $r_0$ and $\theta_0$, *Applied Optics*, 36, 7876, 1996.

5. David L. Fried, TN-110, private communication, 2000. To be submitted to arxiv.org.

6. Fried, D.L., Anisoplanatism in Adaptive Optics, *Journal of the Optical Society of America*, 72, 52-61, 1982

7. Walters D., Scintillation from the RC Optical Telescope, private communication, 2008.

8. Matthias Schöck and Earl J. Spillar, Method for a quantitative investigation of the frozen flow hypothesis, *Journal of the Optical Society of America*, Vol. 17, Issue 9, pp. 1650-1658.

9. Earl Spillar, Marjorie Shoemake, and Ann Slavin, SAM, the Starfire Optical Range Atmospheric Monitor, to be submitted to the *Proceedings of the Astronomical Society of the Pacific*.